

---

01 Apr 2019

## Optical Transportation and Accumulation of Microparticles by Self-Accelerating Cusp Beams

Weiwei Liu

Xiaodong Yang

*Missouri University of Science and Technology, yangxia@mst.edu*

Jie Gao

*Missouri University of Science and Technology, gaojie@mst.edu*

Follow this and additional works at: [https://scholarsmine.mst.edu/mec\\_aereng\\_facwork](https://scholarsmine.mst.edu/mec_aereng_facwork)



Part of the [Mechanical Engineering Commons](#)


---

### Recommended Citation

W. Liu et al., "Optical Transportation and Accumulation of Microparticles by Self-Accelerating Cusp Beams," *Physical Review A*, vol. 99, no. 4, American Physical Society (APS), Apr 2019.

The definitive version is available at <https://doi.org/10.1103/PhysRevA.99.043839>

This Article - Journal is brought to you for free and open access by Scholars' Mine. It has been accepted for inclusion in Mechanical and Aerospace Engineering Faculty Research & Creative Works by an authorized administrator of Scholars' Mine. This work is protected by U. S. Copyright Law. Unauthorized use including reproduction for redistribution requires the permission of the copyright holder. For more information, please contact [scholarsmine@mst.edu](mailto:scholarsmine@mst.edu).

**Optical transportation and accumulation of microparticles by self-accelerating cusp beams**Weiwei Liu, Xiaodong Yang,<sup>\*</sup> and Jie Gao<sup>†</sup>*Department of Mechanical and Aerospace Engineering, Missouri University of Science and Technology, Rolla, Missouri 65409, USA* (Received 28 September 2018; published 29 April 2019)

Most of the self-accelerating beams have monotonous single-channel bending structures, which greatly limit their applications in many fields such as microscopic imaging and particle manipulation. In this paper, the self-accelerating cusp beams with variable numbers of multichannel bending structures are generated to demonstrate the optical transportation and accumulation of micrometer polystyrene particles. The transportation velocity and optical force profiles of the microparticles moving along the bending channels of cusp beams are analyzed. Parallel particle transportation and particle accumulation manipulation from all the bending channels are further demonstrated. These results will inspire a lot of promising applications for self-accelerating beams especially in three-dimensional optical micromanipulation.

DOI: [10.1103/PhysRevA.99.043839](https://doi.org/10.1103/PhysRevA.99.043839)**I. INTRODUCTION**

As one type of the self-accelerating beams, Airy beams were first found in 2007 attributed to the solution of the Schrödinger equation [1,2]. Subsequently, the family of self-accelerating beams has been enriched rapidly accompanied by the discovery of other spatially accelerating solutions of the Maxwell's equations such as Weber beams and Mathieu beams [3–5]. Self-accelerating beams are attractive due to their novel nondiffracting propagation properties and unique bending trajectories, which have enabled numerous applications in microscopic imaging [6–8], generation of curved plasma channels [4,9], nonlinear optics [10], as well as optical particle manipulation [11–13]. Self-accelerating beams with bending optical structures have enabled the three-dimensional (3D) optical manipulation in microfluidics [14–16]. However, conventional self-accelerating beams such as Airy beams only possess monotonous single-channel bending structures [11], which greatly limits their applications in particle manipulation and many other fields. Recently, the emergence of self-accelerating cusp beams has attracted wide attention because of their autofocusing propagation properties and exquisite multiple propagation channel structures [17–19]. Cusp beams are usually derived from the Thom's umbilics [19–22] and will benefit the development of parallel transportation for large numbers of particles in 3D optical manipulation.

In this paper, self-accelerating cusp beams with multichannel bending structures are used to demonstrate optical transportation and accumulation of micrometer polystyrene particles. The cusp beams are generated through the phase modulation with a spatial light modulator (SLM) and coupled into a microscope to conduct 3D optical manipulation. Since the optical intensity distribution along the main lobe of a cusp beam is much smoother than other types of autofocusing beams such as symmetric Airy beams [23,24], the precise transportation of a single particle along the channel of a cusp

beam can be realized. Cusp beams can transport particles within variable numbers of multichannel bending structures by tuning the generating phase profile, which will benefit some optofluidic applications where particle manipulation in different channels is required. Specifically, the transportation velocity and optical force profiles of polystyrene microparticles moving along the bending main lobes of cusp beams are analyzed. Parallel particle transportation and particle accumulation manipulation from all the bending channels are also demonstrated. It can be anticipated that these results will greatly enrich the family of optical micromanipulation configurations and also benefit the development of microfluidics and optofluidics based on the self-accelerating beams.

**II. GENERATION OF CUSP BEAMS**

The generation of the special optical structures of cusp beams can be explained by caustics theory [25,26]. Cusp beams naturally propagate in free space with multiple self-accelerating channels and exhibit multiple high-intensity maxima that are equally spaced along a circle in the transverse dimension. The cusp beam is one kind of self-accelerating beam with a nontrivial morphology and usually does not correspond to those described by standard catastrophe optics [17]. To construct 3D cusp beams, here the Fourier spectra of targeted beams are taken to load in the SLM. The integral representation for the electric field of the cusp beam in Cartesian coordinates can be written as [21]

$$E(x, y, z) = A \int_{-\infty}^{+\infty} \int_{-\infty}^{+\infty} \exp[ik\psi(\xi, \eta, x, y, z)] d\xi d\eta. \quad (1)$$

The phase function in the integral can be written as  $\psi(\xi, \eta, x, y, z) = \phi_m(\xi, \eta) - z(\xi^2 + \eta^2) - (\xi x + \eta y)$ , and  $A$  is a constant and  $k = 2\pi/\lambda$  is the wave number.  $(x, y, z)$  correspond to the coordinates of the cusp beam electric field in the image space, while  $(\xi, \eta)$  are the corresponding spectral variables in the input plane. The generation of cusp beams is realized by the Fourier transform with the phase

<sup>\*</sup>Corresponding author: yangxia@mst.edu<sup>†</sup>Corresponding author: gaojie@mst.edu

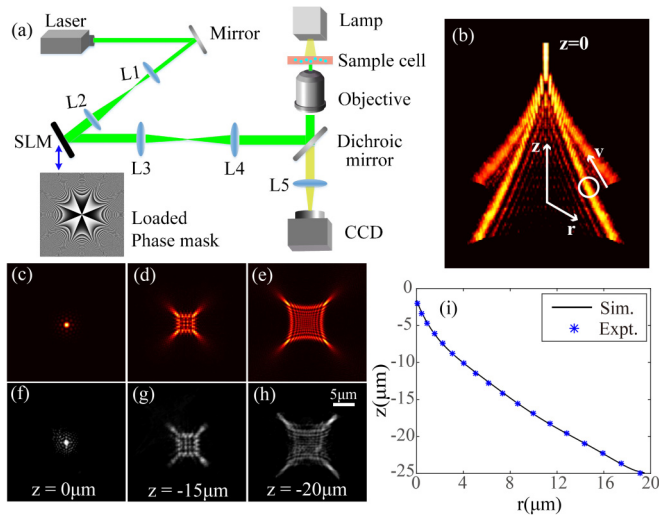


FIG. 1. (a) The typical holographic optical tweezers setup to generate the cusp beam and conduct the optical transportation experiment; the phase mask loaded on the SLM for generating cusp beam with  $m = 4$  is also shown. (b) Schematic of 3D optical transportation by the cusp beam with  $m = 4$ . (c)–(e) Numerical and (f)–(h) measured optical intensity profiles of the cusp beam with  $m = 4$  in the focus plane of the microscope objective lens. (i) The beam deflection of self-accelerating channels for the cusp beam with  $m = 4$  along the propagation in simulation (curve) and experiment (points).  $z$  is the axial coordinate where the origin locates at the autofocusing region of the cusp beam, and  $r$  is the radial coordinate which represents the distance from the center of the beam pattern to a peak in one of the channels of the cusp beam.

term  $\phi_m(\xi, \eta)$  loaded on the SLM. Through a coordinate transformation, the general expression of  $\phi_m(\xi, \eta)$  in polar coordinates can be written as [21]

$$\phi_m(R, \theta) = CR^m \sin(m\theta + w), \quad (2)$$

where  $(R, \theta)$  are the polar variables in the radial and azimuthal directions separately, and  $C$  and  $w$  represent a constant scaling number and the initial phase, respectively. The polynomial order  $m$  determines the number of self-accelerating main lobes of the cusp beam. Here,  $m$  is set as  $m = 3, 4$ , and  $5$  to realize cusp beams with variable channel structures. The typical holographic optical tweezers setup, as shown in Fig. 1(a), is utilized to generate the cusp beam inside the sample cell and conduct the optical transportation experiment. The laser beam at  $532 \text{ nm}$  is first expanded by convex lenses  $L1$  and  $L2$  (focal length  $f_1 = 75 \text{ mm}$ ,  $f_2 = 300 \text{ mm}$ ) and then is incident on the SLM. The convex lenses  $L3$  and  $L4$  ( $f_3 = 200 \text{ mm}$ ,  $f_4 = 150 \text{ mm}$ ) constitute the typical  $4f$  system. The phase profiles loaded on the SLM are specially designed to generate the cusp beams with the appropriate sizes inside the focus region of the microscope objective lens ( $100\times$ , NA 1.3) for transporting microparticles. The lens  $L4$  and the objective lens constitute the conjugate imaging system. A CCD camera with the frame rate up to  $43 \text{ Hz}$  at the screen size of  $680 \times 510$  pixels is used to record the particle motion in the bright field.

Cusp beams possess novel optical pyramid structures during propagation, having the self-accelerating main lobes

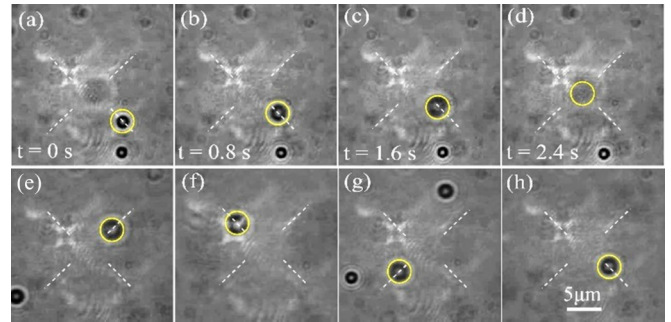


FIG. 2. (a)–(d) The dynamic process of a single particle transported along the self-accelerating channel of the cusp beam with  $m = 4$ . (e)–(h) Single-particle transportation along each channel of the cusp beam in every quadrant. The yellow circle shows the location of the particle transported along the channel of the cusp beam. The dashed lines indicate the transverse position of self-accelerating channels of the cusp beam (media 1 of the Supplemental Material).

which resemble the advanced microscale all-optical channels that are promising for 3D optical manipulation in lab-on-a-chip applications. The cusp beams with  $m = 4$  are first generated to study the dynamic process of the transportation of a single polystyrene microparticle along the bending channels, as shown in Fig. 1(b) with the simulated 3D optical intensity distributions. Compared with other types of autofocusing beams such as symmetric Airy beams, the optical energy distribution along the bending channel of the cusp beam is more continuous and compact in the propagation direction, so that smooth and precise transportation of a single particle along the channel can be realized. Figures 1(c)–1(e) and 1(f)–1(h) present the transverse optical intensity profiles of cusp beams with  $m = 4$  along the axial direction of the microscope objective lens in simulation and experiment, respectively. In simulation, the propagation profiles of cusp beams around the focus of lens  $L3$  are first calculated by the Fourier transform of the transmission angular spectrum of a phase mask loaded on the SLM, and then the beam profiles shown in Fig. 1 at the focus of the objective lens are calculated by multiplying the magnification of the conjugate imaging system of the lens  $L4$  and the objective lens. The position  $z = 0 \mu\text{m}$  in the experiment corresponds to the same transverse section in simulation. It is observed that the four transverse intensity maxima converge into one point along the propagation, indicating the potential convergence effect for particles transported by all the bending channels of the cusp beams. Specifically, Fig. 1(i) shows the deflection of self-accelerating channels of the cusp beam as a function of radial distance in both experiment and simulation. Such a relation between the beam deflection and the transverse position will be applied to derive the 3D location of transported particles.

### III. OPTICAL TRANSPORTATION BY SELF-ACCELERATING CUSP BEAMS

Figures 2(a)–2(d) present the results of optical transportation for a single polystyrene particle with the diameter of  $2 \mu\text{m}$  by the cusp beam with  $m = 4$  along the self-accelerating channel in the fourth quadrant, with the time-sequenced images taken from the recorded video (see Supplemental

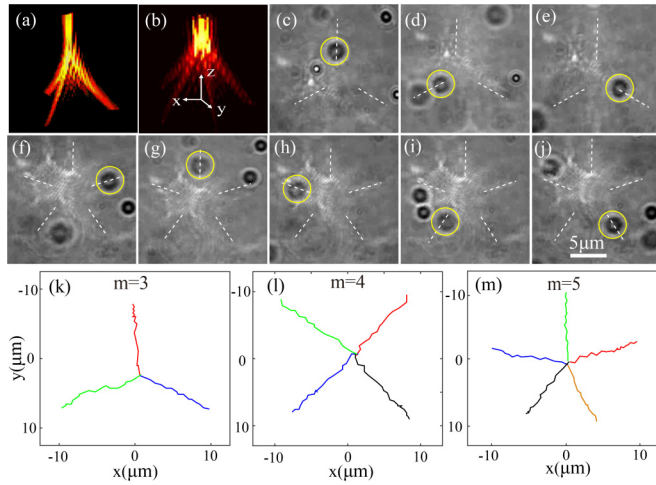


FIG. 3. (a),(b) Simulated 3D optical intensity distributions of cusp beams with  $m = 3$  and  $5$ . Single-particle transportation along all channels of the cusp beams with (c)–(e)  $m = 3$  (media 2 of the Supplemental Material) and (f)–(j)  $m = 5$  (media 3 of the Supplemental Material). (k)–(m) The trajectories of particles transported along the channels of the cusp beams with  $m = 3, 4$ , and  $5$ .

Material [27]) to show the dynamic process of particle motion. The laser power is 60 mW at the entrance pupil of the microscope objective lens. The full width at half maximum (FWHM) of the laser beam in the incident plane of the objective is 4 mm to guarantee the whole optical beam could go through the pupil of the objective to conduct the optical transportation experiment. The energy of the generated cusp beams is distributed around the center of Fig. 2 with the size of about  $25 \times 25 \mu\text{m}^2$ , while the bright areas in the cusp beam images in Fig. 2 are due to the light reflection of the mirrors in the microscopy system, which is not related to the energy contribution of the cusp beam used for the particle's transportation. The particle is suspended in a water solution inside the sample chamber. It is observed that the single particle is transported stably by the bending channel towards the cusp beam center due to the radiation force along the channel, which is similar to the case of Airy beams [11]. Meanwhile, the transported particle also involves the axial motion following the 3D bending channel structure, which is verified by the fact that the images of particles are out of focus during the transportation. Figures 2(e)–2(h) are the images showing the single particle transported by each channel of the cusp beam in every quadrant, indicating the equal transportation capability for all four self-accelerating channels of the cusp beams.

The number of self-accelerating channels for the cusp beam can be varied by tuning the parameter  $m$  in the generating phase profiles. Figures 3(a) and 3(b) show the simulated 3D optical intensity distributions of cusp beams with  $m = 3$  and  $5$ , where similar optical pyramid structures to that of cusp beams with  $m = 4$  are observed, accompanied by the smooth optical energy distributions along self-accelerating channels. The transportation of a single polystyrene particle is also studied for the cusp beams with  $m = 3$  and  $5$ , as shown in Figs. 3(c)–3(e) and 3(f)–3(j), respectively, which are taken from the recorded videos (see Supplemental Material [27]).

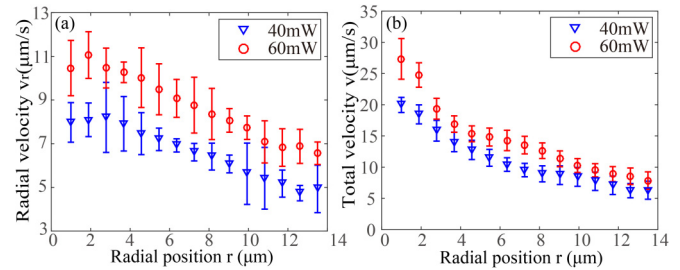


FIG. 4. The measured variations of (a) transverse velocity in the radial direction and (b) total velocity along the 3D beam channel for a single particle as functions of the radial distance by tuning the laser power at 40 and 60 mW.

These beams also stably transport the particles towards the beam center similar to the cusp beam with  $m = 4$ , which indicates that the cusp beams with different number of self-accelerating channels have an equivalent transportation performance for microparticles in 3D optical manipulation. In order to further reflect the particle motion transported by cusp beams, the trajectories of transported particles along the self-accelerating channels for the above three kinds of cusp beams in the transverse direction are also plotted in Figs. 3(k)–3(m). It shows that the particle propulsion along the 3D beam channel is accompanied by slight fluctuations due to Brownian motion, but overall the particles are transported stably to converge towards the beam center of the needlelike optical structure from all-around directions.

#### IV. ANALYSIS OF TRANSPORTATION VELOCITY AND OPTICAL FORCE

Control of a particle conveying velocity in microfluidic channels is the key factor for applications in biological and medical science [28]. Instead of using a micropump in microfluidics, here the particle transportation velocity by cusp beams along their self-accelerating channels can be controlled flexibly by the adjustment of beam energy. In order to quantitatively reflect such velocity regulation and the dynamic motion of transported particles, Figs. 4(a) and 4(b) show the variations of radial velocity  $v_r$  and derived total velocity  $v = \sqrt{v_r^2 + v_z^2}$  as functions of the radial distance by tuning the laser power at 40 and 60 mW, typically along the bending channel in the fourth quadrant of the cusp beam with  $m = 4$ .  $v_r$  is measured based on the tracked transverse locations of particle from the recorded video (see Supplemental Material [27]), while  $v_z$  is derived from the deflection curve in Fig. 1(h), which calibrates the 3D position information of the beam channel and thus the ratio between  $v_r$  and  $v_z$ . Here the particle is expected to move stably along the bending channel of the cusp beam. It is observed that the motion of a single particle along the beam channel is an accelerating process on the whole. Furthermore, higher average transportation velocity along the self-accelerating channels can be achieved by increasing the laser power.

Stable particle transportation by the cusp beam results from the combination of gradient force and radiation pressure within the self-accelerating beam channels. The gradient force will trap the particle and keep it inside the

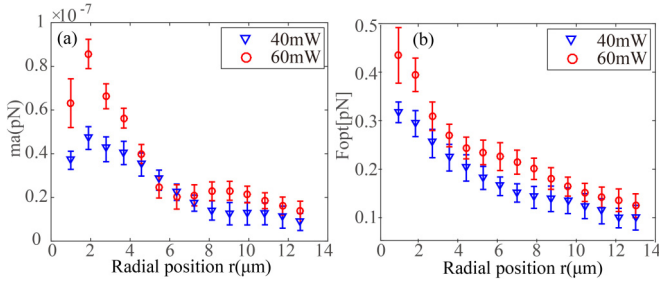


FIG. 5. Variations of (a)  $ma$  and (b)  $F_{\text{opt}}$  as functions of the radial distance in 3D space applied on a single particle by the cusp beam with  $m = 4$  at the laser power of 40 and 60 mW.

bending channel of the cusp beam, while the radiation force  $F_{\text{opt}}$  applied on the polystyrene particle will drive the particle to move along the channel based on Newton's second law of motion,  $F_{\text{opt}} = ma + F_{\text{vis}}$ , where  $m$  and  $a$  are the mass and acceleration of the particle.  $F_{\text{vis}}$  is the viscous force of water for the moving particle as  $F_{\text{vis}} = 6\pi\eta r_0 v$ , where  $r_0$  and  $v$  are the particle radius and the motion velocity, and  $\eta = 0.893 \times 10^{-3} \text{ N s/m}^2$  is the viscosity of water at the room temperature of  $25^\circ\text{C}$  [29]. In the calculation, the  $ma$  term is very small and can be neglected compared to the  $F_{\text{vis}}$  term, so that  $F_{\text{opt}} \approx F_{\text{vis}}$ . Figures 5(a) and 5(b) show the variations of  $ma$  and  $F_{\text{opt}}$  as functions of the radial distance in 3D space. Figure 5(a) clearly shows the dynamic accelerating process of the particle moving along the beam channel, with relatively constant acceleration at the initial stage and then rapidly increased acceleration close to the beam center. Figure 5(b) shows that the optical radiation force for a single particle keeps increasing towards the beam center along the bending channel of the cusp beam, which is consistent with the optical intensity distribution in the self-accelerating channel of a cusp beam [17]. Then the average radiation force applied on the particle is proportional to the laser power. It is noted that the magnitude of the optical force for a single particle is around 1 pN, which indicates the exquisite transportation capability of cusp beams for microscale objects in optical manipulation.

## V. OPTICAL ACCUMULATION OF PARTICLES BY CUSP BEAMS

Distinguished from the precise manipulation of a single particle by the individual channel of the cusp beam, the multichannel structures and autofocusing propagation properties of a cusp beam also provide great advantages in realizing the parallel manipulation of a large number of microscale objects. Here the parallel particle transportation and particle accumulation manipulation from all the bending channels of a cusp beam with different orientations are demonstrated, as shown in Fig. 6. The laser power at the entrance of the microscope objective lens is 50 mW. It is observed that multiple dispersed polystyrene particles at the bottom of the cusp beam [ $\Delta z = 0 \mu\text{m}$ ; Fig. 6(a)] are collected by the multiple bending channels and then lifted up along the beam propagation to a higher position [ $\Delta z = 70 \mu\text{m}$ ; Fig. 6(c)]. Figure 6(b) shows the middle process when the particles are accumulated by the cusp beam. These time-sequenced images are taken from the recorded video (see Supplemental Material [27]). In the

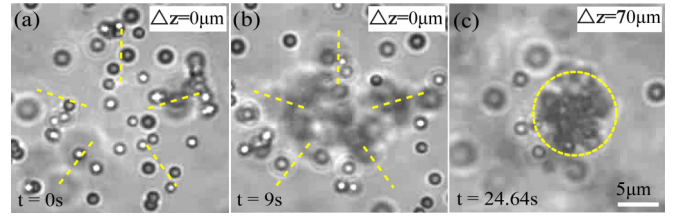


FIG. 6. Optical accumulation of multiple particles by the cusp beam with  $m = 5$  (media 4 of the Supplemental Material).

experiment, the imaging plane of the microscope system is tuned to track the location of multiple particles at the corresponding height. As shown in Fig. 4(b), the transported particles will continue to possess a relatively large velocity as they get across the beam center around the autofocusing region of the cusp beam, and therefore the transported particles actually flow away from the focus so that the accumulation height of the transported multiple particles, shown in Fig. 6(c), will exceed the axial dimension of the cusp beam, which is estimated in Fig. 1(h). However, the particles may also be able to stay at the autofocusing region of the cusp beam when generated with low laser power because there is potentially a trapping area in the autofocusing region, as shown in Ref. [17]. Here, the cusp beams are generated with relatively high laser power to mainly illustrate the particle transportation ability of cusp beams, which could bring different particles or cells to mix together, and may also promote such all-optical beam structure for many biomedical applications. Actually, the transported height for microparticles by cusp beams could be derived from the law of energy conservation. Here we set the transported height of particles by a cusp beam as  $H$ , the function distance of the water viscous force  $F_{\text{vis}}$  acting on the particles is  $H_{\text{vis}}$ , and the function distance of the optical force  $F_{\text{opt}}$  acting on the particles is  $H_{\text{opt}}$ . It is known that the velocities of transported particles at the start and end points during the transportation are both zero. According to the energy conservation law and force analysis for the transported particles, it has  $mgH = F_{\text{opt}}H_{\text{opt}} - F_{\text{vis}}H_{\text{vis}}$ , which gives  $H = (F_{\text{opt}}H_{\text{opt}} - F_{\text{vis}}H_{\text{vis}})/mg$ , indicating that the transported height of microparticles is determined by the above parameters of  $F_{\text{opt}}$ ,  $H_{\text{opt}}$ ,  $F_{\text{vis}}$ ,  $H_{\text{vis}}$  and  $m$ , respectively.

The reason that symmetrical self-accelerating beams such as cusp beams could gather a large amount of microparticles in or out of their autofocusing area is because there exists a large trapping volume around the beam self-focusing region, which has been demonstrated in the previous work [24], while the focused Gaussian beams usually could not gather a number of particles or could only gather a very limited number of particles since their trapping volume is very limited due to the absence of such novel self-focusing beam structures. That is to say, the gathering ability of cusp beams for microparticles is much more efficient than common Gaussian focused beams. Meanwhile, the particle gathering ability of cusp beams is orientation selective, as shown in Fig. 3, because of their variable multichannel beam structures. With the above results, it can be concluded that the generated cusp beams can be used to not only precisely transport single particles in the individual beam channel, but also to manipulate multiple particles simultaneously.

## VI. CONCLUSION

In conclusion, the optical transportation and accumulation of microparticles by self-accelerating cusp beams with variable numbers of multichannel bending structures have been demonstrated. The dynamic process of precise transportation for single particles along the bending channels of cusp beams has been presented, with the analysis of the transportation velocity and optical force for the transported particle in 3D space. As a proof of the parallel transportation functionality of the cusp beam, the particle accumulation for a large number of particles from all the bending channels has

also been realized. These results will not only further enhance 3D optical micromanipulation with complex structured beams for the development of microfluidics and optofluidics, but also greatly inspire many promising applications based on self-accelerating beams.

## ACKNOWLEDGMENTS

The authors acknowledge support from NASA Innovative Advanced Concepts (NIAC) (Grant No. NNX16AL26G) and the Office of Naval Research (Grant No. N00014-16-1-2408).

- 
- [1] G. A. Siviloglou and D. N. Christodoulides, Accelerating finite energy Airy beams, *Opt. Lett.* **32**, 979 (2007).
- [2] G. Siviloglou, J. Broky, A. Dogariu, and D. Christodoulides, Observation of Accelerating Airy Beams, *Phys. Rev. Lett.* **99**, 213901 (2007).
- [3] P. Zhang, Y. Hu, T. Li, D. Cannan, X. Yin, R. Morandotti, Z. Chen, and X. Zhang, Nonparaxial Mathieu and Weber Accelerating Beams, *Phys. Rev. Lett.* **109**, 193901 (2012).
- [4] A. Libster-Hershko, I. Epstein, and A. Arie, Rapidly Accelerating Mathieu and Weber Surface Plasmon Beams, *Phys. Rev. Lett.* **113**, 123902 (2014).
- [5] P. Aleahmad, M.-A. Miri, M. S. Mills, I. Kaminer, M. Segev, and D. N. Christodoulides, Fully Vectorial Accelerating Diffraction-Free Helmholtz Beams, *Phys. Rev. Lett.* **109**, 203902 (2012).
- [6] S. Jia, J. C. Vaughan, and X. Zhuang, Isotropic three-dimensional super-resolution imaging with a self-bending point spread function, *Nat. Photon.* **8**, 302 (2014).
- [7] Y. Lumer, L. Drori, Y. Hazan, and M. Segev, Accelerating Self-Imaging: The Airy-Talbot Effect, *Phys. Rev. Lett.* **115**, 013901 (2015).
- [8] T. Vettenburg, H. I. Dalgarno, J. Nylk, C. Coll-Lladó, D. E. Ferrier, T. Čížmár, F. J. Gunn-Moore, and K. Dholakia, Light-sheet microscopy using an Airy beam, *Nat. Methods* **11**, 541 (2014).
- [9] P. Polynkin, M. Kolesik, J. V. Moloney, G. A. Siviloglou, and D. N. Christodoulides, Curved plasma channel generation using ultraintense Airy beams, *Science* **324**, 229 (2009).
- [10] T. Ellenbogen, N. Voloch-Bloch, A. Ganany-Padowicz, and A. Arie, Nonlinear generation and manipulation of Airy beams, *Nat. Photon.* **3**, 395 (2009).
- [11] D. N. Christodoulides, Optical trapping: Riding along an Airy beam, *Nat. Photon.* **2**, 652 (2008).
- [12] R. Schley, I. Kaminer, E. Greenfield, R. Bekenstein, Y. Lumer, and M. Segev, Loss-proof self-accelerating beams and their use in non-paraxial manipulation of particles' trajectories, *Nat. Commun.* **5**, 5189 (2014).
- [13] P. Zhang, J. Prakash, Z. Zhang, M. S. Mills, N. K. Efremidis, D. N. Christodoulides, and Z. Chen, Trapping and guiding microparticles with morphing autofocusing Airy beams, *Opt. Lett.* **36**, 2883 (2011).
- [14] H. Lee, S. A. Kim, S. Coakley, P. Mugno, M. Hammarlund, M. A. Hilliard, and H. Lu, A multi-channel device for high-density target-selective stimulation and long-term monitoring of cells and subcellular features in *C. elegans*, *Lab Chip* **14**, 4513 (2014).
- [15] C. Yu, F. Tang, X. Qian, Y. Chen, Q. Yu, K. Ni, and X. Wang, Multi-channel microfluidic chip coupling with mass spectrometry for simultaneous electro-sprays and extraction, *Sci. Rep.* **7**, 17389 (2017).
- [16] S. N. Bhatia and D. E. Ingber, Microfluidic organs-on-chips, *Nat. Biotechnol.* **32**, 760 (2014).
- [17] L. Gong, W.-W. Liu, Y.-X. Ren, Y. Lu, and Y.-M. Li, Self-bending symmetric cusp beams, *Appl. Phys. Lett.* **107**, 231110 (2015).
- [18] W. Liu, Y. Zhang, J. Gao, and X. Yang, Generation of three-dimensional optical cusp beams with ultrathin metasurfaces, *Sci. Rep.* **8**, 9493 (2018).
- [19] S. Barwick, Accelerating regular polygon beams, *Opt. Lett.* **35**, 4118 (2010).
- [20] Z. Ren, L. Dong, C. Ying, and C. Fan, Generation of optical accelerating regular triple-cusp beams and their topological structures, *Opt. Express* **20**, 29276 (2012).
- [21] Y. Zhang, Z. Zhang, T. Cheng, Q. Zhang, and X. Wu, Accelerating generalized polygon beams and their propagation, *Chinese Phys. Lett.* **32**, 014205 (2015).
- [22] Y. Zhang, F. Dong, K. Qian, Q. Zhang, W. Chu, X. Ma, and X. Wu, Study on evolving phases of accelerating generalized polygon beams, *Opt. Express* **24**, 5300 (2016).
- [23] P. Vaveliuk, A. Lencina, J. A. Rodrigo, and O. M. Matos, Symmetric Airy beams, *Opt. Lett.* **39**, 2370 (2014).
- [24] W. Liu, Y. Lu, L. Gong, X. Chu, G. Xue, Y. Ren, M. Zhong, Z. Wang, J. Zhou, and Y. Li, Dynamic enhancement of autofocusing property for symmetric Airy beam with exponential amplitude modulation, *J. Opt.* **18**, 075301 (2016).
- [25] A. Zannotti, F. Diebel, M. Boguslawski, and C. Denz, Optical catastrophes of the swallowtail and butterfly beams, *New J. Phys.* **19**, 053004 (2017).
- [26] A. Zannotti, F. Diebel, and C. Denz, Dynamics of the optical swallowtail catastrophe, *Optica* **4**, 1157 (2017).
- [27] See Supplemental Material at <http://link.aps.org/supplemental/10.1103/PhysRevA.99.043839> for the recorded videos displaying the particle transportation and accumulation manipulation by the cusp beams.
- [28] D. J. Beebe, J. S. Moore, J. M. Bauer, Q. Yu, R. H. Liu, C. Devadoss, and B. H. Jo, Functional hydrogel structures for autonomous flow control inside microfluidic channels, *Nature (London)* **404**, 588 (2000).
- [29] G. Pesce, A. Sasso, and S. Fusco, Viscosity measurements on micron-size scale using optical tweezers, *Rev. Sci. Instrum.* **76**, 115105 (2005).